IEEE Access
Multidisciplinary ⋮ Rapid Review ⋮ Open Access Journal

Received February 20, 2022, accepted February 25, 2022, date of publication March 2, 2022, date of current version March 10, 2022.

Digital Object Identifier 10.1109/ACCESS.2022.3155722

Distribution and Attribution of Gross Primary Productivity Increase Over the Mongolian Plateau, 2001-2018

XIAONA CHEN[1,2], XIN TAO[3], (Member, IEEE), AND YAPING YANG[1,2]

[1]National Earth System Science Data Center, State Key Laboratory of Resources and Environmental Information System, Institute of Geographic Sciences and Natural Resources Research, Chinese Academy of Sciences, Beijing 100101, China
[2]Jiangsu Center for Collaborative Innovation in Geographical Information Resource Development and Application, Nanjing 210023, China
[3]Department of Geography, University at Buffalo, Buffalo, NY 14261, USA

Corresponding author: Xiaona Chen (chenxn@igsnrr.ac.cn)

This work was supported in part by the Comprehensive Survey of Biodiversity over the Mongolian Plateau under Grant 2019FY102001; in part by the Branch Center Project of Geography for Resources and Ecology of Knowledge Center, Chinese Engineering Sciences and Technology, under Grant CKCEST-2021-2-10; and in part by the National Earth System Science Data Center (http://www.geodata.cn/).

ABSTRACT Gross primary productivity (GPP) over the Mongolian Plateau (MP) is a vital component of the global terrestrial carbon cycle. Using the latest MODIS GPP estimates at the best achievable spatial resolution along with several ancillary datasets, we investigated GPP variations in the MP region during 2001–2018 and attributed these changes to land-surface temperature (T_s), total precipitation (P_t), land-cover change (LCC), and atmospheric carbon dioxide (CO_2) concentrations. The 18-year-averaged annual cumulative GPP in the MP region was 357.02 ± 24.76 gC m^{-2} yr^{-1} during the study period, ranging from 60.51 ± 6.10 gC m^{-2} yr^{-1} in deserts to 596.41 ± 35.49 gC m^{-2} yr^{-1} in forests. A linear regression analysis indicated a significant overall increase in GPP, at a rate of 3.91 gC m^{-2} yr^{-1} ($p < 0.01$). In comparison, GPP increased at a rate of 0.79 gC m^{-2} yr^{-1} in deserts ($p < 0.01$), 4.79 gC m^{-2} yr^{-1} in forests ($p < 0.01$), and 5.76 gC m^{-2} yr^{-1} in grasslands ($p < 0.01$). Our detailed attribution analysis indicates that GPP is positively sensitive to surface air temperature (0.15 gC °C^{-1}) and total precipitation (0.25 gC mm^{-1}) but negatively sensitive to atmospheric CO_2 concentrations (−0.20 gC mol^{-1}) and LCC (−0.93 gC class^{-1}). Furthermore, we reported large differences in the spatial patterns and magnitudes among individual variables in the GPP attribution analysis, with LCC proving to be the dominant factor followed by CO_2 fertilization effects; climatic factors had comparatively little influence on GPP variations during the study period. Although MODIS GPP does not take CO_2 fertilization effect into account, the close relationship between MODIS GPP and atmospheric CO_2 concentrations still pose referencing value in attributing the GPP increase in this period. Overall, the findings of this study contribute to our understanding of the responses of sensitive ecosystems to the competing effects of climate change and human disturbance at regional scales.

INDEX TERMS Mongolian plateau, gross primary productivity, climate change, driving factors.

I. INTRODUCTION

Terrestrial gross primary productivity (GPP), defined as the carbon uptake by terrestrial ecosystems through plant photosynthesis, is the largest component of the global carbon cycle and a key indicator of land ecosystem dynamics [1]–[3]. GPP is essential for several ecosystem applications, such as crop growth and yield prediction [4], vegetation disturbance monitoring [5], and solar-induced fluorescence retrieval [6] at regional and global scales. As an important part of the East Asian ecosystem, the Mongolian Plateau (MP) not only represents an important ecological barrier in China but also plays an important role in the global carbon cycle [7]. Therefore, accurate information on GPP in this region is vital for both local ecosystem monitoring and global carbon budgeting [8], [9] against the backdrop of a changing climate.

The increasing attention toward patterns and attribution of GPP change in past few years has been driven by the global need for accurate peak carbon and carbon neutral calculations [1]–[3], [8], [9]. Statistical interpolation [10], [11], satellite-based estimation [12], [13], and carbon cycle models [14]–[17] are three widely employed approaches in GPP

The associate editor coordinating the review of this manuscript and approving it for publication was John Xun Yang.

estimation. Compared with statistical interpolation and model simulations, estimation using satellite data has distinct advantages for GPP monitoring, including large spatial coverage, fine spatial resolution, high temporal resolution, and economic and practical in application. Several published GPP datasets are currently available [12], [13], [18], *e.g.*, the Moderate Resolution Imaging Spectroradiometer (MODIS) [12] and Global Land Surface Satellite (GLASS) [13] datasets. Although GPP estimates from carbon models and satellite observations show similar patterns at a global scale, there are large differences in the temporal trends, seasonality, and interannual variability of GPP calculated from individual regional and local datasets because of varying inputs and forcing mechanisms [1], [19]. In addition, due to the lack of observational GPP data over the MP, accurate estimation in this region remains difficult, and high-quality GPP datasets are crucially needed.

Among the published satellite-retrieved estimates, the good performance of MODIS GPP, based on a light-use efficiency algorithm, has been highlighted. The validation of GPP calculated from ground sites and MODIS-based estimates shows good spatiotemporal correlation [10], [11], [20]. Moreover, the newly released gap-filled MODIS GPP estimates (MOD17A2HGF) Version 6 [21] provide spatially complete GPP data at a 500-m spatial resolution, offering new opportunities for regional-scale studies.

In addition to studies of GPP variability, the attribution of GPP anomalies has recently gained significant attention. Several putative drivers have been attributed to GPP changes including surface air temperature (T_s) [22], precipitation (P_t) [23], [24], atmospheric carbon dioxide (CO_2) concentrations [25], [26], aerosol optical depth (AOD) [27], plant phenology and physiology [28], and land-cover change (LCC) [25]. Generally, increases in atmospheric CO_2 concentrations dominate GPP changes via CO_2 fertilization effects; the T_s and P_t produce similar but lower-magnitude positive GPP effects; solar radiation (R_s) is associated with an overall decrease in GPP; and LCC is positively correlated with GPP [25]. However, the mechanisms underlying regional-scale GPP attribution remain debated. The putative driving factors of large-scale variability in GPP are determined by location and biome type. For example, AOD is positively correlated with GPP in forests but negatively correlated with GPP in grasslands over China [27]. Furthermore, although the sensitivity of GPP to LCC is positive at a global scale, a negative effect is observed in the rainforests of South America and Eurasia [25]. Although attribution analyses have been carried out at different scales, the relative contributions of different drivers of GPP change remain highly uncertain [25], [29], especially at regional scales.

Affected by the Siberia-Mongolia High in winter, the East Asian Monsoon in summer, and the westerly circulation, the MP is extremely fragile and ecologically sensitive to climate variations [30], [31]. Under the competing effects of climate change and human activity, the MP has experienced drastic ecosystem shifts over the past several decades including grassland degradation [32], forest decline [33], cooling effects from re-vegetation [34], and the rapid loss of lakes [35]. Nevertheless, evidence of GPP variability in this region remains limited. To address this gap, here we investigate the pattern of GPP changes in the MP region and its drivers using the latest MODIS GPP simulations from 2001 to 2018. We specifically focus on the relationships between GPP and four major putative drivers (T_s, P_t, CO_2 concentration, and LCC) and their underlying forcing mechanisms. Results in this study provide valuable evidence of GPP change and its underlying mechanisms in this globally important region, having implications for global carbon budgets as well as understanding ecosystem sensitivities and responses to climate change and human disturbance.

II. DATA AND METHODS

A. STUDY AREA

Due to its arid and semi-arid climate, habitats of the MP transition from deserts to grasslands and forests, from southwest to northeast [31]. As rapid climate and land-cover changes in this region may have a marked impact on GPP, we attributed GPP variability in grasslands, forests, and deserts according to the global terrestrial ecoregions classification developed by the Nature Conservancy (TNC) [36], as shown in Figure 1.

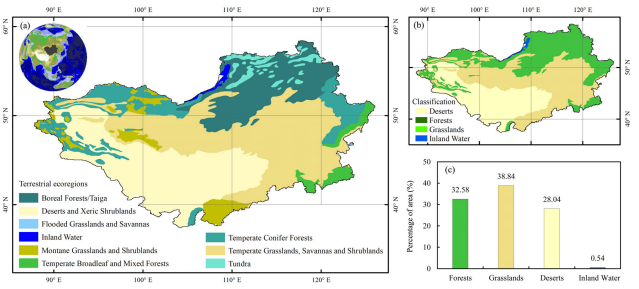

FIGURE 1. Location of the Mongolian Plateau (MP) showing (a) terrestrial ecoregions, (b) general land-cover types, and (c) area covered by each land-cover type (%) according to the Nature Conservancy classification.

According to the TNC classification, the MP is covered by nine ecoregions, which were re-classified into forests, grasslands, and deserts to facilitate statistical analysis. The ''forests'' classification included temperate conifer forests, temperate broadleaf and mixed forests, boreal forests/taiga, and tundra; the ''grasslands'' category included montane grasslands and shrublands, flooded grasslands and savannas, as well as temperate grasslands, savannas, and shrublands; and the ''deserts'' category included deserts and xeric shrublands. Forests are mostly distributed in mountainous areas, including the Altay Mountains in the west, the Khangai Mountains in the west, and the Khentii Mountains in the north, which account for 32.58% of the total study area. Grasslands are distributed in the middle of the MP and account for 38.84% of the total area. Finally, deserts are located in the southwest of the MP and account for 28.04% of the total area. Although the deserts in the north of the region

are more arid, they receive some precipitation in summer and support sparse vegetation that contributes to GPP.

B. DATASETS

We used the latest satellite-based MODIS GPP dataset and datasets of major putative drivers covering the period from 2001 to 2018.

1) GPP DATASETS

To capture the spatial pattern and assess interannual variability and long-term trends in GPP, eight-day composite gap-filled MOD17A2HGF data [21] with a 500-m spatial resolution were downloaded from the National Aeronautics and Space Administration (NASA) Land Processes Distributed Active Archive Center (https://lpdaac.usgs.gov/products/mod17a2hgfv006/).

MODIS GPP was the first satellite-based modeled GPP dataset for monitoring global vegetation productivity with complete spatial coverage and high spatial resolution. To ensure data quality, poor-quality inputs from the eight-day Fraction of Photosynthetically Active Radiation and Leaf Area Index have been removed from the MOD17A2HGF dataset based on the quality control flag for each grid cell.

2) LAND-COVER DATASET

To attribute GPP changes to LCC, we employed the annual International Geosphere-Biosphere Programme (IGBP) classification from the Terra and Aqua combined MODIS yearly land-cover dataset (MCD12Q1) with a 500-m spatial resolution. This dataset covers 17 IGBP categories encompassing 11 natural vegetation categories, three land-use and land-mosaic categories, and three vegetation-free land categories [37]. For the purpose of our study, the land-cover data were analyzed in a 0.10° grid, in which all 500-m pixels encompassed in the 0.10° cells were used to calculate the proportions of the dominant land-cover types.

3) ATMOSPHERIC CO_2 CONCENTRATION DATASET

To attribute GPP changes to atmospheric CO_2 concentrations, we used the Carbon Tracker CT2019B product, providing global monthly continuous spatial surface-atmosphere flux of atmospheric CO_2 concentrations. CT2019B is distributed by the Global Monitoring Laboratory (GML) of the National Oceanic and Atmospheric Administration (NOAA), and is based on observations from the NOAA Earth System Research Laboratories (ESRL) greenhouse gas observational network and collaborating institutions (spatial resolution = 1.0°) [38]. In this dataset, terrestrial biosphere, wildfire, fossil fuel emissions, atmospheric transport, and other factors are assimilated to estimate atmospheric CO_2 mole fractions.

4) REANALYSIS TEMPERATURE AND PRECIPITATION DATASET

Previous studies have reported that climatic factors are closely related to GPP changes at a regional scale [22]–[24]. To attribute GPP changes to local meteorological variables, we employed monthly averaged 2-m surface air temperature (T_s) and total precipitation (P_t) datasets with a resolution of 0.10° (approximately 9 km) from the European Center for Medium Range Weather Forecasts (ECMWF) Reanalysis v5-Land (ERA5-Land) [39]. These data are widely considered suitable for ground-level modeling [40]–[42]. Compared with other ERA5 reanalysis data, ERA5-Land offers more accurate classifications of land parameters and land status.

5) SOLAR RADIATION DATASET

Incoming solar radiation (R_s) is the energy source for photosynthesis and causes changes in T_s, relative humidity, and evaporation, and thus, indirectly affects plant productivity [43]. Therefore, R_s is the one of the most important environmental factors affecting terrestrial ecosystem productivity and carbon budgets. Here, to explore whether changes in R_s are associated with GPP anomalies over the MP, we employed the Clouds and the Earth's Radiant Energy System (CERES) Energy Balanced and Filled (EBAF) dataset [44] (spatial resolution = 1.0°).

6) DATA PREPARATION

All of the used datasets are summarized in Table 1.

TABLE 1. Summary of datasets used in this study.

Variable	Dataset	Timespan	Temporal resolution	Spatial resolution
GPP	MOD17A2 HGF	2001–2018	8-day	500 m
CO_2 concentration	CT2019B	2001–2018	Monthly	1.0°
Land cover	MCD12Q1	2001–2018	Yearly	500 m
T_s P_t	ERA5-Land	2001–2018	Monthly	0.1°
R_s	CERES	2001–2018	Monthly	1.0°

Prior to analysis, all the gridded datasets were resampled to gridcells with a spatial resolution of 0.10° in geographic projection. Using "gdalwarp" software (https://gdal.org/programs/gdalwarp.html), datasets with a spatial resolution coarser than 0.10° were regridded using the "cubic-spline" function; datasets with spatial resolution finer than 0.10° were regridded using the "average" function.

C. RELATIVE CONTRIBUTION CALCULATION

The influences of four putative drivers on GPP (T_s, P_t, atmospheric CO_2 concentration, and LCC) were analyzed in detail using multiple linear regression analysis [45], [46]. To avoid multicollinearity among the four drivers, we employed ridge regression. First, each driver was normalized to facilitate cross-comparison between variables with different units and scales. For variable X_i, the z-score (X_{iz}) was calculated using Equation (1) [47]:

$$X_{iz} = \frac{X_i - \mu_X}{\delta_X}, \tag{1}$$

where X_{iz} is the normalized variable X_i, μ_x is the mean value of variable X_i, and δ_x is the standard deviation of variable X_i.

Second, ridge regression analysis was carried out to calculate the sensitivity of GPP to the four putative drivers using Equation (2):

$$GPP_z = \sum_{i=1}^{n} \beta_i \times X_{iz} + \alpha, \tag{2}$$

where GPP_z is the z-score-normalized GPP; X_{iz} is the normalized putative driver X_i; β_i is the standard ridge regression coefficient for putative driver X_i; α is the residual error, representing the contribution of unknown factors to GPP, such as fire, pests, wind, and disease; and n is the number of putative drivers.

Third, the relative contributions of the putative drivers to GPP variability were obtained using the ridge regression coefficients and the z-score series of each driver, as follows:

$$\eta_{ci} = \beta_i \times X_{iz}, \tag{3}$$

where η_{ci} is the contribution of putative driver X_i to the z-score-normalized GPP variation, X_{iz} is the z-score-normalized X_i, and β_i is the linear slope of X_{iz}.

Finally, the relative contribution (η_{rc}) of each individual putative driver to GPP was confirmed using Equation (4):

$$\eta_{rci} = \frac{|\eta_{ci}|}{|\eta_{c1}| + |\eta_{c2}| + \cdots + |\eta_{cn}|}, \tag{4}$$

where η_{rci} is the relative contribution of X_i to GPP change, and n is the number of putative drivers.

Ridge regression analysis is an effective approach for solving collinearity problems between independent variables [48] and has been successfully applied in GPP trend analysis of the 'Three North' region of China (northeastern, northern, and northwestern regions) [46] and Yellow River Basin [49].

III. RESULTS

In the subsequent subsections, changes in GPP over the MP are first described for the period 2001–2018. Then, concurrent changes in the four putative drivers are described. Finally, the results of attribution analysis are presented.

A. CHANGES IN GPP OVER THE MP

The spatial pattern of the 18-year-averaged (2001–2018) annual cumulative GPP over the MP is displayed in Figure 2, as calculated from the MOD17A2HGF dataset.

With the transition from desert to forest, GPP generally increases from the southwest to northeast parts of the MP (Figure 2a). For the 2001–2018 study period, the overall 18-year average annual cumulative GPP of the MP was estimated to be 357.02 ± 24.76 gC m^{-2} yr^{-1}. However, large differences were identified among the individual biome types, with the annual cumulative GPP of forests, grasslands, and deserts calculated as 596.41 ± 35.49, 386.07 ± 37.95, and 60.51 ± 6.10 gC m^{-2} yr^{-1}, respectively.

The fluctuations in annual cumulative GPP ranged between 317.31 gC m^{-2} yr^{-1} (in 2003) and 410.92 gC m^{-2} yr^{-1} (in 2018). Over the entire study period, the linear regression analysis indicated a significant increase in annual cumulative GPP at a rate of 3.91 gC m^{-2} yr^{-1} ($p < 0.01$); in deserts, forests, and grasslands, the rate of increase was 0.79 ($p < 0.01$), 4.79 ($p < 0.01$), and 5.76 gC m^{-2} yr^{-1} ($p < 0.01$).

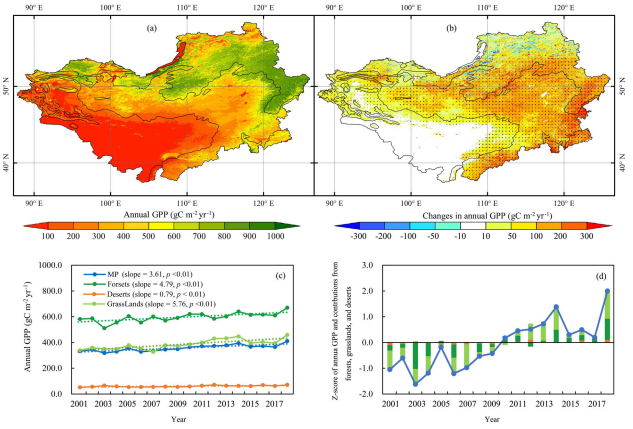

FIGURE 2. Spatial distribution of (a) 18-year-averaged (2001–2018) annual cumulative gross primary productivity (GPP) over the Mongolian Plateau (MP) and (b) associated change during this period. (c) Interannual variations in annual cumulative GPP over the MP among different biome types for the same period. (d) Contributions of different biome types to GPP changes in MP during the study period.

The observed GPP increase was strongest in the southeastern part of the MP, coinciding with the grasslands in this region [50]. Moreover, forests, grasslands, and deserts accounted for 39.94%, 53.72%, and 6.44% of the overall change in GPP during the study period.

B. CHANGES IN METEOROLOGICAL VARIABLES OVER THE MP

Changes in T_s and P_t are shown in Figure 3 for the 2001–2018 study period, as calculated from the latest ERA5-land atmospheric reanalysis dataset.

The spatial pattern of annual mean T_s exhibited a decreasing trend from south to north over the MP (Figure 3a). The changes in T_s exhibited a conspicuous warming trend in grasslands and deserts areas (Figure 3b) compared to a cooling trend in the northwest part of the MP, which is consistent with the reported Eurasian cooling caused by a strengthening Siberian High [51].

Compared with T_s, P_t (Figure 3c) and associated overall changes during the study period (Figure 3d) exhibited larger spatial differences within the study area. The 18-year averaged annual-mean P_t showed an increasing trend from the deserts in the southwest to the forests in the northeast. P_t showed an increasing trend in the eastern MP but decreased at the southern and northern margins of the MP. Notably, changes in P_t were opposite to the Palmer Drought Severity Index (PDSI) anomalies in this region during the 2000s [52].

The detailed changes in annual-mean T_s and P_t are summarized in Table 2.

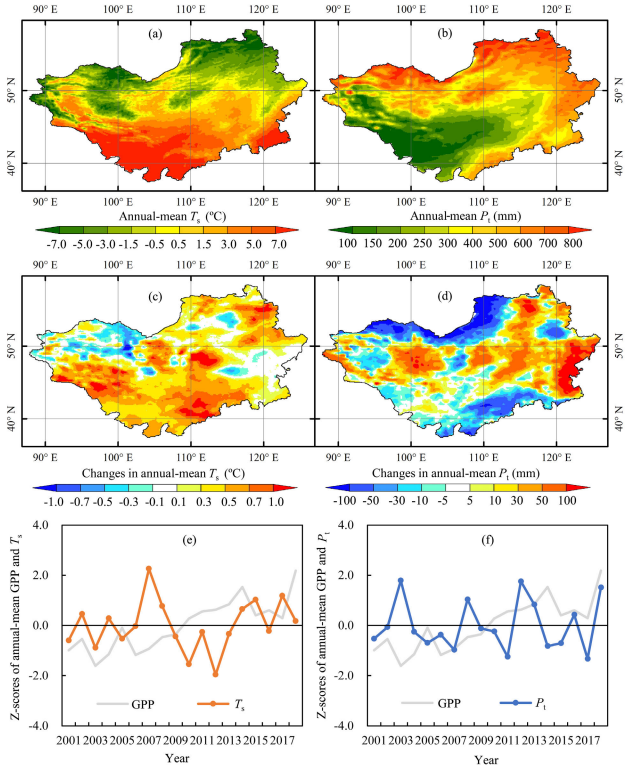

FIGURE 3. Distribution of 18-year averaged (2001–2018) annual-mean (a) T_s and (b) P_t over the Mongolian Plateau (MP) and overall change in (c) T_s and (d) P_t during the study period. Z-scores of (e) gross primary productivity (GPP) and T_s, and (f) GPP and P_t, during the study period.

TABLE 2. Changes in T_S (°C) and P_t (mm), and their linear correlations (r) with gross primary productivity (GPP) over the Mongolian Plateau (MP) for the period 2001–2018.

Regions	T_s		P_t	
	change	r	change	r
MP	0.45	-0.05	0.13	0.10
Forests	0.22	0.16	-4.63	0.26
Grasslands	0.24	-0.23	17.39	0.45 (*)
Deserts	0.44	-0.29	-3.21 (**)	0.52 (**)

Significance levels: *0.10; **0.05; other correlations were not significant at the 0.10 level.

In most regions, the changes in T_s and P_t were insignificant, except for the desert regions. In deserts, P_t decreased by −3.21 mm between 2001 and 2018, which was positively correlated with the increase in GPP in this region ($r = 0.52$, $p < 0.05$). In addition, although grassland P_t showed an insignificant increasing trend between 2001 and 2018, this was positively correlated with GPP changes ($r = 0.45$, $p < 0.10$).

C. CHANGES IN ATMOSPHERIC CO_2 CONCENTRATION AND LAND COVER

The spatial pattern of 18-year-averaged atmospheric CO_2 concentrations and the dominant land-cover types over the MP are shown in Figure 4.

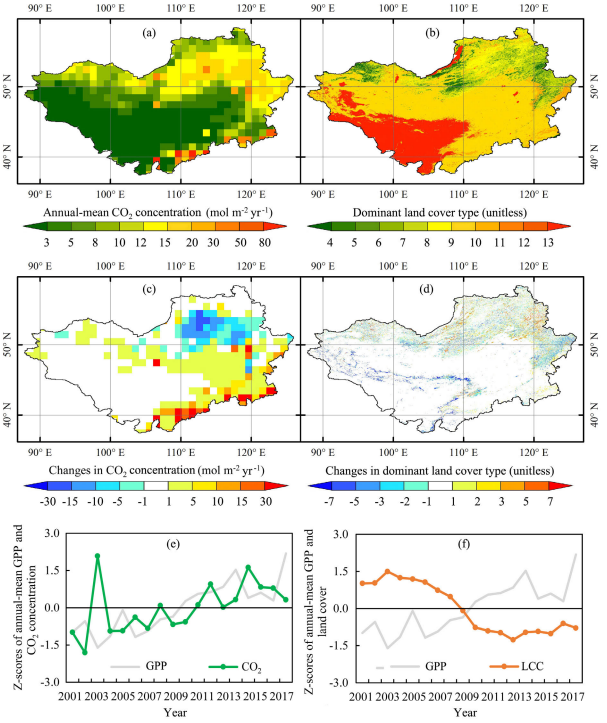

FIGURE 4. Distribution of 18-year annual-mean (a) atmospheric CO_2 concentration and (b) dominant land-cover types and overall change in (c) atmospheric CO_2 concentration and (d) dominant land-cover types in the Mongolian Plateau (MP) region during the period 2001–2018. Z-scores of (e) gross primary productivity (GPP) and atmospheric CO_2 concentration, and (f) GPP and dominant land-cover types during the study period.

Influenced by the intensity of human activity in the MP region, atmospheric CO_2 concentrations are high in Inner Mongolia relative to lower values in the southwestern deserts (Figure 4a). The dominant land-cover types exhibit a remarkable spatial transition from the deserts in the southwest to the grasslands in the central area and the forests in the northeast (Figure 4b).

The linear regression analyses revealed a significant increase in atmospheric CO_2 concentrations in the MP region between 2001 and 2018 (1.99 mol m^{-2}, $p < 0.05$). Notable regional differences were revealed, however, with significant decreases in the northeast forest region and increases in the grassland regions, especially at the southern margin. These changes are similar to the decrease in CO_2 concentrations previously reported in this region for the period between 2009 and 2018 [53]. The dominant land-cover types exhibited a decreasing trend during the study period (−0.11 class^{-1}, $p < 0.05$), indicating an overall transition from desert to grassland and from grassland to forest. As shown in Figure 4d, the most remarkable changes have occurred near the transition regions between deserts and grasslands, which corroborates the findings reported by Jiang *et al.* [34].

The observed changes in annual-mean atmospheric CO_2 concentrations and the dominant land-cover types during the study period are detailed in Table 3.

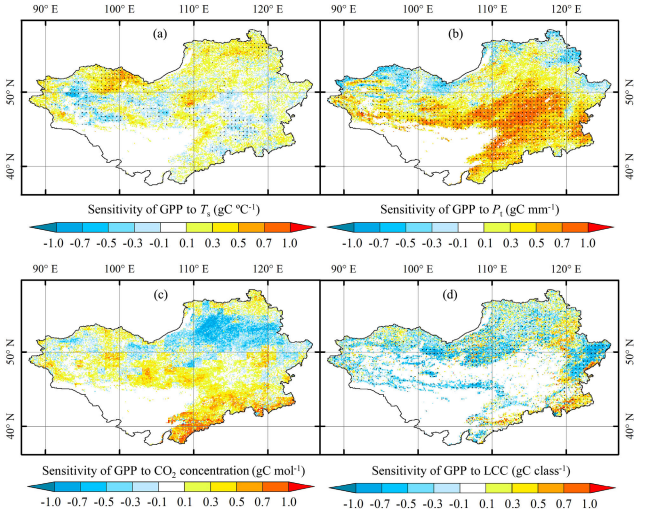

FIGURE 5. Sensitivity of annual cumulative gross primary productivity (GPP) to changes in (a) T_s (gC °C^{-1}), (b) P_t (gC mm^{-1}), (c) CO_2 concentration (gC mol^{-1}), and (d) land-cover class (LCC) (gC class^{-1}) over the Mongolian Plateau (MP) during the period 2001–2018.

As shown in Table 3, atmospheric CO_2 concentrations over grassland and desert areas increased at rates of 4.83 ($p < 0.05$) and 0.68 mol m^{-2}($p < 0.05$) between 2001 and 2018. Moreover, atmospheric CO_2 was highly correlated with annual GPP augmentation in the forest ($r = -0.54$, $p < 0.05$), grassland ($r = 0.72$, $p < 0.05$), and desert ($r = 0.68$, $p < 0.05$) areas.

In comparison to CO_2 concentration, the dominant land-cover types in the forest, grassland, and desert areas showed an overall decreasing trend, with rates of -0.10 ($p < 0.05$), -0.04 ($p < 0.05$), and -0.23 ($p < 0.05$), respectively. These trends were negatively correlated with annual GPP variability in these regions, with r corresponding values to -0.58 ($p < 0.05$), -0.71 ($p < 0.05$), and -0.81 ($p < 0.05$), respectively.

D. ATTRIBUTION ANALYSIS

The changes in annual cumulative GPP over the MP during the period 2001–2018 and their sensitivities to individual putative drivers, calculated using Equation (3), are shown in Figure 5.

Annual cumulative GPP shows a conspicuous rising trend in the central and southeastern regions of the MP (Figure 2b), and this is positively correlated with increases in T_s (Figure 5a) and atmospheric CO_2 concentrations (Figure 5c) in these regions. As shown in Figure 5d, the evident LCC decrease is also associated with the increase in GPP at the eastern margin of the MP.

Detailed ridge regression coefficients reveal that GPP change was positively correlated with T_s (0.1495 gC °C^{-1}) and P_t (0.2424 gC mm^{-1}) but negatively correlated with atmospheric CO_2 concentration (-0.1993 g C mol^{-1}) and LCC (-0.9348 gC class^{-1}) during the 2001–2018 study period. However, there were large differences among the desert, grassland, and forest land-cover categories.

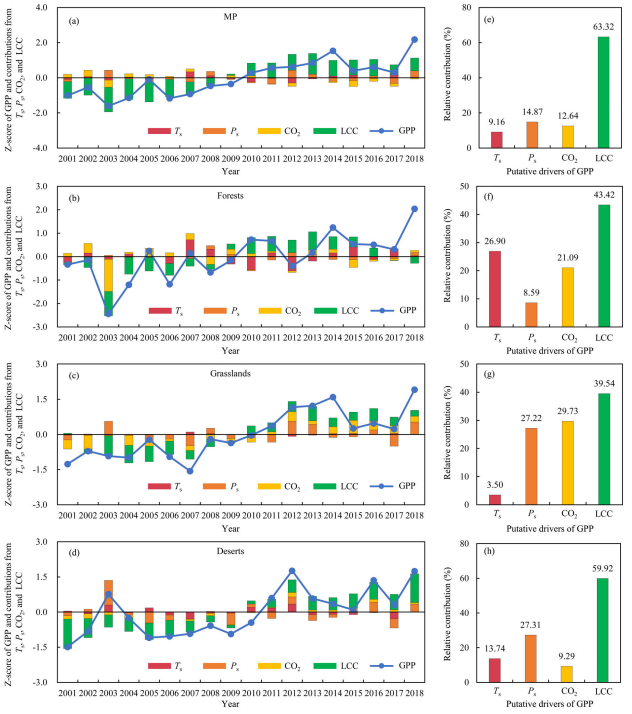

FIGURE 6. Relative contributions of different putative drivers to annual cumulative gross primary productivity (GPP) changes over the (a) entire Mongolian Plateau (MP), (b) forest areas, (c) grassland areas, and (d) desert areas for the period 2001–2018.

TABLE 3. Changes in atmospheric CO_2 concentration (mol m^{-2}) and land cover class (LCC), and their linear correlations (r) with annual gross primary productivity (GPP) over the Mongolian Plateau (MP) during the period 2001–2018.

Regions	CO_2 concentration		LCC	
	change	r	change	r
MP	1.99 (**)	0.27	-0.11 (**)	-0.85(**)
Forests	-0.21	-0.54 (**)	-0.10 (**)	-0.58 (**)
Grasslands	4.83 (**)	0.72 (**)	-0.04 (**)	-0.71 (**)
Deserts	0.68 (**)	0.65 (**)	-0.23 (**)	-0.81 (**)

Significance levels: *0.10; **0.05; other correlations were not significant at the 0.10 level.

For example, annual cumulative GPP was negatively correlated to atmospheric CO_2 concentration (-0.3958 gC mol^{-1}) in forests but significantly and positively correlated with grasslands (0.3247 gC mol^{-1}) and deserts (0.1101 gC mol^{-1}) over the same period.

The relative contributions of each putative driver to GPP anomalies as calculated from Equation (4) are shown in Figure 6; the contributions of T_s, P_t, atmospheric CO_2 concentration, and LCC over the entire MP were 9.16%, 14.87%, 12.64%, and 63.32% for the period 2001–2018, respectively.

Notably, our analysis revealed large-scale spatial differences in the relative contributions of each putative driver to GPP changes in forest, grassland, and desert areas. The contributions from T_s, P_t, atmospheric CO_2 concentration, and LCC were 26.90%, 8.59%, 21.09%, and 43.42% for

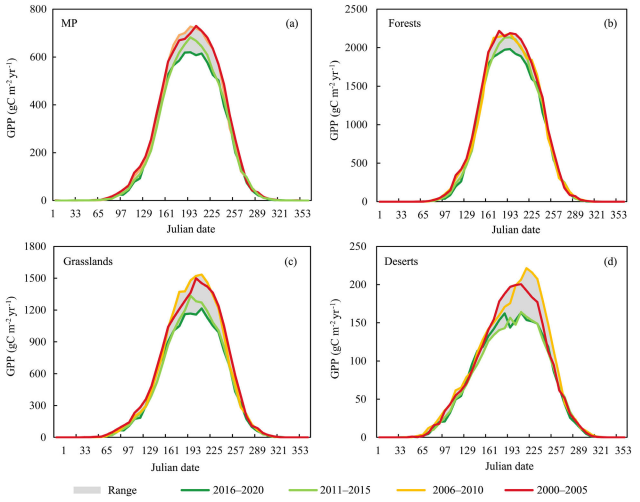

FIGURE 7. Interannual variations in eight-day cumulative gross primary productivity (GPP) over the (a) entire Mongolian Plateau (MP) and (b) forest, (c) grassland, and (d) desert regions during the period 2001–2018.

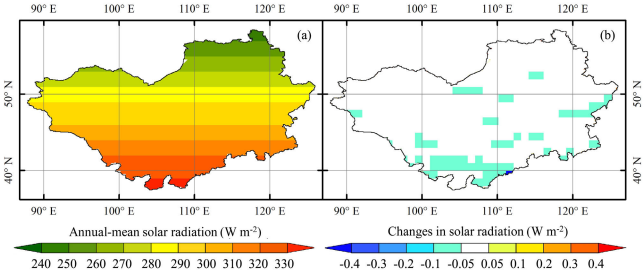

FIGURE 8. Distribution of 18-year annual-mean (a) R_S and (b) its associated changes during 2001–2018.

forests; 3.50%, 27.22%, 29.73%, and 39.54% for grasslands; and 13.74%, 27.31%, 9.29%, and 59.92% for deserts, respectively.

IV. DISCUSSION

A. INTERANNUAL VARIATION IN GPP

According to Sun *et al*. [25] and Alexandrov [54], an increase in both the amplitude of the GPP seasonal cycle and in growing season length can lead to elevated GPP.

To comprehensively analyze the reasons for observed GPP increases in the MP region, we mapped eight-day seasonal variations in cumulative GPP for the entire region based on four sub-periods (2001–2005, 2006–2010, 2011–2015, and 2016–2018), as shown in Figure 7.

Notably, the multi-year averaged annual GPP for the earlier (2001–2010) and latter (2011–2018) sub-periods showed a remarkable change in amplitude (height of peaks in Figure 7a) whereas changes in growing season length were negligible (width of peaks in Figure 7a). We also found similar patterns for the amplitudes of the GPP seasonal cycle in forest (Figure 7b), grassland (Figure 7d), and desert (Figure 7e). Based on this, we suggest that changes in the length of the growing season can be excluded from the attribution of GPP changes during our study period.

B. CHANGES IN SOLAR RADIATION

Previous studies have shown that R_S changes significantly in response to AOD anomalies, which may lead to GPP changes [27] and [55]. To explore whether R_S changes Contributed to the observed increase in GPP in the MP region, we mapped the 18-year annual mean R_S and its associated overall change in Figure 8.

Between 2001 and 2018, the 18-year averaged annual mean R_S in the MP region was 293.31 ($\pm$ 0.12) W m^{-2}, with a clear latitudinal gradation from south to north (Figure 8a). However, overall changes during the study period were minimal (Figure 8b). Detailed statistical analysis showed that the regions with R_S changes between -0.05 and 0.05 W m^{-2} and between -0.10 and -0.05 W m^{-2} account for 89% and 11% of the study area, respectively. This indicated that R_s had little influence on annual GPP variability during the study period, and thus, could be excluded from the attribution analysis.

C. UNCERTAINTY ANALYSIS

Global terrestrial GPP has increased by 31 $\pm$ 5% since 1900, driven by the effects of a changing climate and increasing atmospheric CO_2 concentrations on several ecosystem processes including vegetation productivity, harvesting, deforestation, and secondary forest regrowth [29]. However, the patterns of GPP changes in terrestrial ecosystems demonstrate high spatial variability because of the coupled interactions between vegetation characteristics and environmental variables, *e.g.,* rising atmospheric CO_2 concentrations, changing land cover, AOD, and climatic variability [2], [25], [27].

Satellite-based GPP estimates have been considered highly reliable because of the advantages they offer, with respect to consistent spatial and temporal information on vegetation dynamics. Compared with other satellite-based and model-simulated GPP estimates, the MOD17A2HGF product has proven a feasible and useful means of evaluating GPP in the MP region. We observed a remarkable increase in GPP in this region between 2001 and 2018, and this has partly coincided with enhanced net CO_2 uptake by terrestrial and marine ecosystems, as reported for the period 1959–2010 [56]. Nevertheless, our results differ from recent reports suggesting that there has been no proportional augmentation in terrestrial gross carbon sequestration from enhanced greening of the Earth's surface [57]. Moreover, in contrast to the findings of Zhou *et al*. [28], our analysis reveals a remarkable increase in the amplitude of the seasonal GPP cycle rather than an increase in the length of the growing season. Therefore, we excluded phenological shifts from our attribution analysis.

Previous work has indicated that atmospheric CO_2 concentration is the dominant factor driving global GPP increases between 1982 and 2015 [25]. However, our attribution analysis revealed that LCC dominated the GPP changes in the MP region over the last few decades, which contrasts with

the findings of regional- and global-scale GPP attribution studies by Sun *et al*. [25] and Zhang *et al*. [27]. Since MOD17A2HGF does not take CO_2 fertilization effect into account, the MOD17A2HGF-based analysis on CO_2 fertilization effect is not valid. However, the close relationship between MOD17A2HGF and atmospheric CO_2 concentrations still pose referencing value in attributing the GPP increase in this period. Furthermore, as shown in Figure 4d, land-cover change has dominated the transition between desert and grassland, and between grassland and forest, in the MP region, with GPP showing a significant and sensitivity to LCC in these regions. In addition, although we found that P_t has not been the dominant factor affecting GPP change overall, it has played a key role in the grassland area of the MP region. This is corroborated by findings of Yuan *et al*. [24], suggesting that P_t plays an important role in GPP dynamics in the grasslands of northern China. Moreover, different from the general global rising trend, atmospheric CO_2 concentrations have decreased in the forested areas of MP, and this has been negatively correlated with the increase in GPP across the region. This is not unexpected, as CO_2 fertilization only partially accounts for changes in GPP, as reported by Keenan *et al*. [58].

V. SUMMARY AND CONCLUSION

The estimation and attribution of GPP changes are of great significance for understanding regional terrestrial carbon cycling, the response of vegetation to climate change and human activity, and for assessing ecosystem health. Using satellite-based and model ensemble GPP estimates and several ancillary datasets, we mapped the pattern of annual GPP over the MP and explored its associations with both climate change and human activity indicators. Our results help fill the current gap in GPP studies in the MP region and can inform future regional-scale terrestrial ecosystem studies.

Using the latest MODIS GPP dataset, we found a general increase in GPP in the MP region from southwest to northeast, with remarkable spatial variability among forest, grassland, and desert areas between 2000 and 2018. Overall, our linear regression analysis indicates that annual GPP has shown a significant increase during this period, at a rate of 3.91 gC m^{-2} yr^{-1} ($p < 0.01$). Based on multiple datasets, we attribute these trends to climatic factors, LCC, and atmospheric CO_2 concentrations, with LCC accounting for 63.32% of the observed increase followed by atmospheric CO_2 concentration (12.64%). In comparison, we suggest that climatic factors have had a limited influence on the GPP increase in the MP region during this period.

Distinguishing the effects of climate, LCC, and atmospheric CO_2 concentrations not only provides valuable insight into the impacts of future climate change on productivity, but also reveals the ecological consequences of ongoing LCC and rising CO_2 concentrations. As such, in addition to being relevant to the MP region, our results can inform local-scale GPP studies in inland arid and semi-arid regions, as well as provide additional motivation for mitigating the negative impacts of ongoing human activity and future climate change.

REFERENCES

[1] M. Chen *et al.*, "Regional contribution to variability and trends of global gross primary productivity," *Environ. Res. Lett.*, vol. 12, no. 10, Sep. 2017, Art. no. 105005.

[2] C. Beer *et al.*, "Terrestrial gross carbon dioxide uptake: Global distribution and covariation with climate," *Science*, vol. 329, pp. 834–838, Aug. 2010.

[3] N. You, J. Meng, L. Zhu, S. Jiang, L. Zhu, F. Li, and L. Kuo, "Isolating the impacts of land use/cover change and climate change on the GPP in the Heihe River Basin of China," *J. Geophys. Res., Biogeosci.*, vol. 125, no. 10, Oct. 2020.

[4] K. Guan, J. A. Berry, Y. Zhang, J. Joiner, L. Guanter, G. Badgley, and D. B. Lobell, "Improving the monitoring of crop productivity using spaceborne solar-induced fluorescence," *Global Change Biol.*, vol. 22, no. 2, pp. 716–726, Feb. 2016.

[5] N. G. McDowell *et al.*, "Global satellite monitoring of climate-induced vegetation disturbances," *Trends Plant Sci.*, vol. 20, pp. 114–123, Feb. 2015.

[6] P. Gentine and S. H. Alemohammad, "Reconstructed solar-induced fluorescence: A machine learning vegetation product based on MODIS surface reflectance to reproduce GOME-2 solar-induced fluorescence," *Geophys. Res. Lett.*, vol. 45, no. 7, pp. 3136–3146, Apr. 2018.

[7] S. Tong, Q. Lai, J. Zhang, Y. Bao, A. Lusi, Q. Ma, X. Li, and F. Zhang, "Spatiotemporal drought variability on the Mongolian Plateau from 1980–2014 based on the SPEI-PM, intensity analysis and Hurst exponent," *Sci. Total Environ.*, vol. 615, pp. 1557–1565, Feb. 2018.

[8] K. B. Tokarska, M. B. Stolpe, S. Sippel, E. M. Fischer, C. J. Smith, F. Lehner, and R. Knutti, "Past warming trend constrains future warming in CMIP6 models," *Sci. Adv.*, vol. 6, no. 12, Mar. 2020, Art. no. eaaz9549.

[9] H. D. Matthews, K. B. Tokarska, Z. R. J. Nicholls, J. Rogelj, J. G. Canadell, P. Friedlingstein, T. L. Frölicher, P. M. Forster, N. P. Gillett, T. Ilyina, R. B. Jackson, C. D. Jones, C. Koven, R. Knutti, A. H. MacDougall, M. Meinshausen, N. Mengis, R. Séférian, and K. Zickfeld, "Opportunities and challenges in using remaining carbon budgets to guide climate policy," *Nature Geosci.*, vol. 13, no. 12, pp. 769–779, Nov. 2020.

[10] H. Zhu, A. Lin, L. Wang, Y. Xia, and L. Zou, "Evaluation of MODIS gross primary production across multiple biomes in China using eddy covariance flux data," *Remote Sens.*, vol. 8, no. 5, p. 395, May 2016.

[11] M. He, Y. Zhou, W. Ju, J. Chen, L. Zhang, S. Wang, N. Saigusa, R. Hirata, S. Murayama, and Y. Liu, "Evaluation and improvement of MODIS gross primary productivity in typical forest ecosystems of East Asia based on eddy covariance measurements," *J. Forest Res.*, vol. 18, no. 1, pp. 31–40, Feb. 2013.

[12] S. W. Running, R. R. Nemani, F. A. Heinsch, M. Zhao, M. Reeves, and H. Hashimoto, "A continuous satellite-derived measure of global terrestrial primary production," *BioScience*, vol. 54, pp. 547–560, Jun. 2004.

[13] W. Yuan, S. Liu, G. Zhou, G. Zhou, L. L. Tieszen, D. Baldocchi, C. Bernhofer, H. Gholz, A. H. Goldstein, M. L. Goulden, D. Y. Hollinger, Y. Hu, B. E. Law, P. C. Stoy, T. Vesala, and S. C. Wofsy, "Deriving a light use efficiency model from eddy covariance flux data for predicting daily gross primary production across biomes," *Agricult. Forest Meteorol.*, vol. 143, nos. 3–4, pp. 189–207, Apr. 2007.

[14] M. Dury, A. Hambuckers, P. Warnant, A. Henrot, E. Favre, M. Ouberdous, and L. François, "Responses of European forest ecosystems to 21st century climate: Assessing changes in interannual variability and fire intensity," *iForest-Biogeosci. Forestry*, vol. 4, no. 2, pp. 82–99, Apr. 2011.

[15] H. Tian, G. Chen, C. Lu, X. Xu, D. J. Hayes, W. Ren, S. Pan, D. N. Huntzinger, and S. C. Wofsy, "North American terrestrial CO_2 uptake largely offset by CH_4 and N_2O emissions: Toward a full accounting of the greenhouse gas budget," *Climatic Change*, vol. 129, nos. 3–4, pp. 413–426, Mar. 2014.

[16] A. Bondeau, P. C. Smith, S. Zaehle, S. Schaphoff, W. Lucht, W. Cramer, D. Gerten, H. Lotze-Campen, C. Müller, M. Reichstein, and B. Smith, "Modelling the role of agriculture for the 20th century global terrestrial carbon balance," *Global Change Biol.*, vol. 13, no. 3, pp. 679–706, Mar. 2007.

[17] M. Guimberteau *et al.*, "ORCHIDEE-MICT (v8.4.1), a land surface model for the high latitudes: Model description and validation," *Geosci. Model Develop.*, vol. 11, no. 1, pp. 121–163, Jan. 2018.

[18] J. Wang, R. Sun, H. Zhang, Z. Xiao, A. Zhu, M. Wang, T. Yu, and K. Xiang, "New global MuSyQ GPP/NPP remote sensing products from 1981 to 2018," *IEEE J. Sel. Topics Appl. Earth Observ. Remote Sens.*, vol. 14, pp. 5596–5612, 2021.

[19] R. A. Feagin *et al.*, "Tidal wetland gross primary production across the continental United States, 2000–2019," *Global Biogeochem. Cycles*, vol. 34, Jan. 2020, Art. no. e2019GB006349.

[20] S. Plummer, "On validation of the MODIS gross primary production product," *IEEE Trans. Geosci. Remote Sens.*, vol. 44, no. 7, pp. 1936–1938, Jul. 2006.

[21] S. Running and M. Zhao, "MOD17A2HGF MODIS/terra gross primary productivity gap-filled 8-day L4 global 500 m SIN grid V006," NASA EOSDIS Land Processes DAAC, Sioux Falls, SD, USA, Tech. Rep., 2019, doi: 10.5067/MODIS/MOD17A2HGF.006.

[22] N. Madani, N. C. Parazoo, J. S. Kimball, A. P. Ballantyne, R. H. Reichle, M. Maneta, S. Saatchi, P. I. Palmer, Z. Liu, and T. Tagesson, "Recent amplified global gross primary productivity due to temperature increase is offset by reduced productivity due to water constraints," *AGU Adv.*, vol. 1, no. 4, Dec. 2020, Art. no. e2020AV000180.

[23] M. Berkelhammer, I. C. Stefanescu, J. Joiner, and L. Anderson, "High sensitivity of gross primary production in the rocky mountains to summer rain," *Geophys. Res. Lett.*, vol. 44, no. 8, pp. 3643–3652, Apr. 2017.

[24] W. Yuan *et al.*, "Multiyear precipitation reduction strongly decreases carbon uptake over Northern China," *J. Geophys. Res., Biogeosci.*, vol. 119, no. 5, pp. 881–896, May 2014.

[25] Z. Sun, X. Wang, H. Yamamoto, H. Tani, G. Zhong, S. Yin, and E. Guo, "Spatial pattern of GPP variations in terrestrial ecosystems and its drivers: Climatic factors, CO_2 concentration and land-cover change, 1982–2015," *Ecol. Informat.*, vol. 46, pp. 156–165, Jul. 2018.

[26] S. Wang *et al.*, "Recent global decline of CO_2 fertilization effects on vegetation photosynthesis," *Science*, vol. 370, pp. 1295–1300, Dec. 2020.

[27] J. Zhang, J. Ding, J. Zhang, M. Yuan, P. Li, Z. Xiao, C. Peng, H. Chen, M. Wang, and Q. Zhu, "Effects of increasing aerosol optical depth on the gross primary productivity in China during 2000–2014," *Ecol. Indicators*, vol. 108, Jan. 2020, Art. no. 105761.

[28] S. Zhou, Y. Zhang, K. K. Caylor, Y. Luo, X. Xiao, P. Ciais, Y. Huang, and G. Wang, "Explaining inter-annual variability of gross primary productivity from plant phenology and physiology," *Agricult. Forest Meteorol.*, vols. 226–227, pp. 246–256, Oct. 2016.

[29] V. Haverd, B. Smith, J. G. Canadell, M. Cuntz, S. Mikaloff-Fletcher, G. Farquhar, W. Woodgate, P. R. Briggs, and C. M. Trudinger, "Higher than expected CO_2 fertilization inferred from leaf to global observations," *Global Change Biol.*, vol. 26, no. 4, pp. 2390–2402, Feb. 2020.

[30] R. John, J. Chen, Z.-T. Ou-Yang, J. Xiao, R. Becker, A. Samanta, S. Ganguly, W. Yuan, and O. Batkhishig, "Vegetation response to extreme climate events on the Mongolian Plateau from 2000 to 2010," *Environ. Res. Lett.*, vol. 8, no. 3, Aug. 2013, Art. no. 035033.

[31] C. Lu, H. Tian, J. Zhang, Z. Yu, S. Pan, S. Dangal, B. Zhang, J. Yang, N. Pederson, and A. Hessl, "Severe long-lasting drought accelerated carbon depletion in the Mongolian Plateau," *Geophys. Res. Lett.*, vol. 46, no. 10, pp. 5303–5312, May 2019.

[32] J. Wang, H. Wei, K. Cheng, A. Ochir, D. Davaasuren, P. Li, F. K. Shun Chan, and E. Nasanbat, "Spatio-temporal pattern of land degradation from 1990 to 2015 in Mongolia," *Environ. Develop.*, vol. 34, Jun. 2020, Art. no. 100497.

[33] G. Duveiller, J. Hooker, and A. Cescatti, "The mark of vegetation change on earth's surface energy balance," *Nature Commun.*, vol. 9, no. 1, p. 679, Feb. 2018.

[34] H. Jiang, N. Lu, X. Zhang, L. Yao, and Y. Bai, "Satellite observed cooling effects from re-vegetation on the Mongolian Plateau," *Sci. Total Environ.*, vol. 781, Aug. 2021, Art. no. 146707.

[35] S. Tao, J. Fang, X. Zhao, S. Zhao, H. Shen, H. Hu, Z. Tang, Z. Wang, and Q. Guo, "Rapid loss of lakes on the Mongolian Plateau," *Proc. Nat. Acad. Sci. USA*, vol. 112, no. 7, pp. 2281–2286, Feb. 2015.

[36] TNC. *Terrestrial Ecoregional Boundaries and Assessments Geodatabase*. Accessed: Jan. 15, 2021. [Online]. Available: http://conserveonline.org/workspaces/ecoregional.shapefile

[37] M. A. Friedl, D. Sulla-Menashe, B. Tan, A. Schneider, N. Ramankutty, A. Sibley, and X. Huang, "MODIS collection 5 global land cover: Algorithm refinements and characterization of new datasets," *Remote Sens. Environ.*, vol. 114, no. 1, pp. 168–182, Jan. 2010.

[38] A. R. Jacobson *et al.*, "CarbonTracker CT2019B," NOAA Global Monit. Lab., 2020, doi: 10.25925/20201008.

[39] S. J. Muñoz. *ERA5-Land Monthly Averaged Data From 1981 to Present*. Accessed: Jan. 15, 2021. [Online]. Available: https://cds.climate.copernicus.eu/cdsapp#!/dataset/10.24381/cds.68d2bb30?tab=overview

[40] E. L. Wipfler, K. Metselaar, J. C. van Dam, R. A. Feddes, E. van Meijgaard, L. H. van Ulft, B. van den Hurk, S. J. Zwart, and W. G. M. Bastiaanssen, "Seasonal evaluation of the land surface scheme HTESSEL against remote sensing derived energy fluxes of the transdanubian region in Hungary," *Hydrol. Earth Syst. Sci.*, vol. 15, no. 4, pp. 1257–1271, Apr. 2011.

[41] G. Balsamo, A. Beljaars, K. Scipal, P. Viterbo, B. van den Hurk, M. Hirschi, and A. K. Betts, "A revised hydrology for the ECMWF model: Verification from field site to terrestrial water storage and impact in the integrated forecast system," *J. Hydrometeorol.*, vol. 10, no. 3, pp. 623–643, Jun. 2009.

[42] J. Muñoz-Sabater, E. Dutra, A. Agustí-Panareda, C. Albergel, G. Arduini, G. Balsamo, S. Boussetta, M. Choulga, S. Harrigan, H. Hersbach, B. Martens, D. G. Miralles, M. Piles, N. J. Rodríguez-Fernández, E. Zsoter, C. Buontempo, and J.-N. Thépaut, "ERA5-land: A state-of-the-art global reanalysis dataset for land applications," *Earth Syst. Sci. Data*, vol. 13, no. 9, pp. 4349–4383, Sep. 2021.

[43] R. Moazenzadeh, B. Mohammadi, S. Shamshirband, and K.-W. Chau, "Coupling a firefly algorithm with support vector regression to predict evaporation in Northern Iran," *Eng. Appl. Comput. Fluid Mech.*, vol. 12, no. 1, pp. 584–597, Jun. 2018.

[44] N. G. Loeb, D. R. Doelling, H. Wang, W. Su, C. Nguyen, J. G. Corbett, L. Liang, C. Mitrescu, F. G. Rose, and S. Kato, "Clouds and the earth's radiant energy system (CERES) energy balanced and filled (EBAF) top-of-atmosphere (TOA) edition-4.0 data product," *J. Climate*, vol. 31, no. 2, pp. 895–918, Jan. 2018.

[45] X. Chen, X. Mo, S. Hu, and S. Liu, "Contributions of climate change and human activities to ET and GPP trends over North China Plain from 2000 to 2014," *J. Geograph. Sci.*, vol. 27, no. 6, pp. 661–680, Mar. 2017.

[46] S. Xie, X. Mo, S. Hu, and S. Liu, "Contributions of climate change, elevated atmospheric CO_2 and human activities to ET and GPP trends in the Three-North Region of China," *Agricult. Forest Meteorol.*, vol. 295, Dec. 2020, Art. no. 108183.

[47] E. Kreyszig, *Advanced Engineering Mathematics*. Jefferson City, MO, USA: Wiley, 1979, pp. 1014–1015.

[48] E. Walker and J. B. Birch, "Influence measures in ridge regression," *Technometrics*, vol. 30, no. 2, pp. 221–227, May 1988.

[49] T. Pei, X. Wu, X. Li, Y. Zhang, F. Shi, Y. Ma, P. Wang, and C. Zhang, "Seasonal divergence in the sensitivity of evapotranspiration to climate and vegetation growth in the Yellow River Basin, China," *J. Geophys. Res., Biogeosci.*, vol. 122, no. 1, pp. 103–118, Jan. 2017.

[50] L. Miao, Z. Sun, Y. Ren, F. Schierhorn, and D. Müller, "Grassland greening on the Mongolian Plateau despite higher grazing intensity," *Land Degradation Develop.*, vol. 32, no. 2, pp. 792–802, Jan. 2021.

[51] B. Li, Y. Li, Y. Chen, B. Zhang, and X. Shi, "Recent fall Eurasian cooling linked to North Pacific sea surface temperatures and a strengthening Siberian high," *Nature Commun.*, vol. 11, no. 1, p. 5202, Oct. 2020.

[52] C. Lu, H. Tian, J. Zhang, Z. Yu, S. Pan, S. Dangal, B. Zhang, J. Yang, N. Pederson, and A. Hessl, "Severe long-lasting drought accelerated carbon depletion in the Mongolian Plateau," *Geophys. Res. Lett.*, vol. 46, no. 10, pp. 5303–5312, May 2019.

[53] M. Sheng, L. Lei, Z.-C. Zeng, W. Rao, and S. Zhang, "Detecting the responses of CO_2 column abundances to anthropogenic emissions from satellite observations of GOSAT and OCO-2," *Remote Sens.*, vol. 13, no. 17, p. 3524, Sep. 2021.

[54] G. A. Alexandrov, "CMIP6 simulations of GPP growth satisfy the constraint imposed by increasing CO_2 seasonal-cycle amplitude," *IOP Conf. Ser., Earth Environ. Sci.*, vol. 606, Nov. 2020, Art. no. 012003.
[55] M. Wild, "Global dimming and brightening: A review," *J. Geophys.*, vol. 114, Oct. 2009, Art. no. D00D16.
[56] A. P. Ballantyne, C. B. Alden, J. B. Miller, P. P. Tans, and J. W. White, "Increase in observed net carbon dioxide uptake by land and oceans during the past 50 years," *Nature*, vol. 488, pp. 2–70, Aug. 2012.
[57] Y. Zhang, C. Song, L. E. Band, and G. Sun, "No proportional increase of terrestrial gross carbon sequestration from the greening earth," *J. Geophys. Res., Biogeosci.*, vol. 124, no. 8, pp. 2540–2553, Aug. 2019.
[58] T. F. Keenan, X. Luo, M. G. De Kauwe, B. E. Medlyn, I. C. Prentice, B. D. Stocker, N. G. Smith, C. Terrer, H. Wang, Y. Zhang, and S. Zhou, "A constraint on historic growth in global photosynthesis due to increasing CO_2," *Nature*, vol. 600, no. 7888, pp. 253–258, Dec. 2021.

XIAONA CHEN received the M.S. degree in cartography and geographical information system from the Chinese Academy of Sciences, Beijing, China, in 2010, and the Ph.D. degree in cartography and geographical information system from Beijing Normal University, Beijing, in 2016.

She is currently an Associate Professor with the State Key Laboratory of Resources and Environmental Information System, Institute of Geographic Sciences and Natural Resources Research, Chinese Academy of Sciences. Her research interests include climate change, vegetation dynamics, and remote sensing.

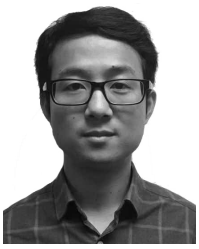

XIN TAO (Member, IEEE) received the Ph.D. degree in geography from the University of Maryland, College Park, MD, USA.

He is currently a Clinical Assistant Professor with the Department of Geography, University at Buffalo, USA. His research interests include the estimation of bio-geophysical variables from satellite data, the data fusion of satellite products, and the scaling effect and scale transformation of bio-geophysical variables.

YAPING YANG received the B.S. degree in economic administration from the National Academy of Governance of China, Beijing, in 2003.

She is currently a Senior Engineer with the Institute of Geographic Sciences and Natural Resources Research, Chinese Academy of Sciences, and the Director of the National Earth System Science Data Center of China. She has been engaged in the research and practice of Earth data science and informatization in scientific research for several years. Her research interests include data integration and data mining.